# Non-Hermitian doping of epsilon-near-zero media

Marino Coppolaro[a], Massimo Moccia[a], Giuseppe Castaldi[a], Nader Engheta[b,1], and Vincenzo Galdi[a,1]

[a]Fields & Waves Lab, Department of Engineering, University of Sannio, I-82100 Benevento, Italy; and [b]Department of Electrical and Systems Engineering, University of Pennsylvania, Philadelphia, PA 19104-6314

Edited by George C. Schatz, Northwestern University, Evanston, IL, and approved May 7, 2020 (received for review January 19, 2020)

**In solid-state physics, "doping" is a pivotal concept that allows controlling and engineering of the macroscopic electronic and optical properties of materials such as semiconductors by judiciously introducing small concentrations of impurities. Recently, this concept has been translated to two-dimensional photonic scenarios in connection with host media characterized by vanishingly small relative permittivity ("epsilon near zero"), showing that it is possible to obtain broadly tunable effective magnetic responses by introducing a single, nonmagnetic doping particle at an arbitrary position. So far, this phenomenon has been studied mostly for lossless configurations. In principle, the inevitable presence of material losses can be compensated via optical gain. However, taking inspiration from quantum (e.g., parity–time) symmetries that are eliciting growing attention in the emerging fields of non-Hermitian optics and photonics, this suggests considering more general gain–loss interactions. Here, we theoretically show that the photonic doping concept can be extended to non-Hermitian scenarios characterized by tailored distributions of gain and loss in either the doping particles or the host medium. In these scenarios, the effective permeability can be modeled as a complex-valued quantity (with the imaginary part accounting for the gain or loss), which can be tailored over broad regions of the complex plane. This enables a variety of unconventional optical responses and waveguiding mechanisms, which can be, in principle, reconfigured by varying the optical gain (e.g., via optical pumping). We envision several possible applications of this concept, including reconfigurable nanophotonics platforms and optical sensing, which motivate further studies for their experimental validation.**

metamaterials | ENZ | non-Hermitian optics | epsilon-near-zero | doping

In optics and photonics, the fast-paced progress in the science and technology of artificial materials and metamaterials (1, 2) has granted access to unusual effective material properties that are not necessarily available in nature. Among these, especially interesting and promising are certain extreme-parameter regimes where the effective relative permittivity and/or permeability are vanishingly small. For these regimes, which include the epsilon-near-zero (ENZ) and near-zero-index cases, a plethora of exotic phenomena have been demonstrated, such as tunneling through deformed waveguides (3); geometry-invariant resonators (4); bound states in the continuum (5–7); and enhanced nonlinear (8, 9), nonreciprocal (10), and quantum (11) effects. The reader is also referred to refs. 12–14. and references therein for recent reviews and perspectives.

In a recent study (15), Liberal et al. put forward the intriguing concept of "photonic doping" of ENZ media. Specifically, they demonstrated that a single two-dimensional (2D), nonmagnetic doping particle embedded in an ENZ host medium could be exploited to tailor the effective permeability of the medium over a broad range of positive and negative values, while preserving the ENZ character, irrespective of the particle position. This enables, for instance, the engineering of extreme parameter responses, such as perfectly magnetic conductors and epsilon-and-mu-near-zero, without the need of magnetic material constituents. These results, validated experimentally at microwave frequencies (with a near-cutoff waveguide mimicking the ENZ host medium), have paved the way for new exciting developments in reconfigurable and flexible photonics (16), nonlinear (9, 17) and nonreciprocal (17, 18) optics, and quantum (19) and transformation-invariant (20) metamaterials.

In the original investigation above, attention was mainly focused on the ideal lossless case, although one may intuitively think of exploiting active (gain) constituents to compensate for the unavoidable losses. In fact, the interplay between gain and loss may have far-reaching implications that extend well beyond the mere compensation. Within this framework, quantum mechanics concepts such as parity–time (PT) symmetry (21) have inspired new directions and perspectives in the tailoring of gain–loss interactions. The newly established and thought-provoking fields of non-Hermitian optics and photonics (22–24) have enlarged the conventional constitutive parameter space of interest to the entire complex plane, with losses not necessarily considered as detrimental effects, but rather instrumental to attain anomalous light–matter interactions, including, for example, exceptional points (25, 26), negative refraction (27), unidirectional cloaking (28), and spectral singularities (29).

Non-Hermitian optics concepts are particularly intriguing in ENZ media, where the effects of relatively low levels of loss and/or gain can be dramatically enhanced (30–32). For instance, recent studies have demonstrated a variety of interesting effects including tunneling (33), waveguiding (34), coherent perfect absorption (35), immunity to impurities (36), exceptional points and spectral singularities (37, 38), and nonlinear and nonreciprocal effects (17).

Against this background, here we theoretically explore the non-Hermitian doping of ENZ media. Specifically, we study two scenarios: 1) non-Hermitian dopants, in the form of nonmagnetic core–shell cylindrical particles (with loss in the core and gain in

## Significance

**The recently introduced concept of photonic doping in epsilon-near-zero media enables the tailoring and control of the effective magnetic response over broad regions of the parameter space, by resorting to a limited number of arbitrarily placed, nonmagnetic doping particles. Here, we theoretically extend this idea to non-Hermitian scenarios with either doping particles or host media characterized by tailored distributions of gain and loss. This considerably enlarges the attainable effective permeability parameter space, granting access to the entire complex plane. In this extended vision, losses are not considered as second-order, detrimental effects, and their interplay with gain is instrumental to enabling several intriguing effects of potential interest in reconfigurable nanophotonics and optical sensing, whose practical implementation is deferred to future studies.**

Author contributions: G.C., N.E., and V.G. designed research; M.C., M.M., G.C., and V.G. performed research; M.C., M.M., G.C., N.E., and V.G. analyzed data; and N.E. and V.G. wrote the paper.

The authors declare no competing interest.

This article is a PNAS Direct Submission.



[1]To whom correspondence may be addressed. Email: engheta@seas.upenn.edu or vgaldi@unisannio.it.

This article contains supporting information online at https://www.pnas.org/lookup/suppl/doi:10.1073/pnas.2001125117/-/DCSupplemental.

the shell, or vice versa), embedded in an ENZ host medium; and 2) dielectric cylindrical doping particles embedded in a non-Hermitian (PT-symmetric) ENZ host medium. For the first scenario, we show that it is possible to tailor the parameters so as to induce a resonant phenomenon that yields large tunability (both in sign and amplitude) of the effective permeability over the entire complex plane. This enables, for instance, some interesting reconfigurability mechanisms for which the system can be switched from impedance-matched (epsilon-and-mu-near-zero) to strongly mismatched responses via small variations of the gain. Other interesting responses include realizing sensible signal amplification in conjunction with near-zero reflection or transmission. For the second scenario, we show that photonic doping can be effectively exploited to enhance and control certain waveguiding phenomena that can occur at a gain–loss interface, in the presence of very small gain–loss levels.

The above theoretical findings promise to significantly enlarge the applicability of the photonic doping concept, and may open up intriguing directions in reconfigurable and flexible photonics, as well as optical sensing scenarios. Their experimental validation requires further studies.

## Results

**Basic Idea and Theory.** We start considering the 2D problem geometry in Fig. 1*A*, consisting of an arbitrarily shaped host region filled by an ENZ medium (with relative permittivity $\varepsilon_h$), doped with a core–shell cylindrical particle with interior and exterior radii $R_i$ and $R_e$, and corresponding relative permittivities $\varepsilon_i$ and $\varepsilon_e$, respectively. All materials are nonmagnetic ($\mu = 1$), and the entire structure is embedded in vacuum. Throughout our study, we assume transversely magnetic polarized excitation (with $z$-directed magnetic field) and implicit $\exp(-i\omega t)$ time-harmonic dependence, with geometry and field quantities invariant along the $z$ direction.

The ENZ host medium can be described via a Drude-type model,

$$\varepsilon_h(\omega) = 1 - \frac{\omega_{ph}^2}{\omega(\omega + i\Gamma_h)}, \qquad [1]$$

with $\omega_{ph}$ and $\Gamma_h$ denoting the plasma radian frequency and collision factor, respectively. As experimentally demonstrated in ref. 15, at microwave frequencies, such behavior can be mimicked by a near-cutoff waveguide. At higher (e.g., terahertz and optical) frequencies, reliance could be made on naturally occurring ENZ materials such as silicon carbide (39) and indium tin oxide (40) which, however, tend to exhibit sensible losses (see also the general discussion in ref. 41). Nevertheless, loss-compensated or even slightly active ENZ materials can be, in principle, attained via composite materials featuring plasmonic waveguides embedded in a gain medium (37) or plasmonic nanoshells with quantum dots (42). In what follows, we assume that losses in the ENZ host are negligible or somehow compensated, so that the assumption $\varepsilon_h \approx 0$ underlying the general theory in ref. 15 holds.

For the core (lossy) material, we consider instead a standard Lorentz–Drude model,

$$\varepsilon_i(\omega) = \hat{\varepsilon}_i - \frac{\omega_{pi}^2}{(\omega^2 - \omega_{0i}^2 + i\omega\Gamma_i)}, \qquad [2]$$

with $\hat{\varepsilon}_i$, $\omega_{0i}$, and $\Gamma_i$ being the high-frequency limit, center radian frequency, and collision factor, respectively. Finally, for the gain medium, we assume a standard approximate linearized model (43) for dielectric materials doped with fluorescent dye molecules (modeled as four-level atomic systems), namely,

$$\varepsilon_e(\omega) = \hat{\varepsilon}_e + \frac{\sigma_a}{(\omega^2 + i\Delta\omega_a\omega - \omega_a^2)} \frac{(\tau_{21} - \tau_{10})\Gamma_p\overline{N}_0}{\left[1 + (\tau_{32} + \tau_{21} + \tau_{10})\Gamma_p\right]}, \qquad [3]$$

where $\omega_a$ denotes the emitting radian frequency, $\Delta\omega_a$ is the bandwidth of the dye transition, $\hat{\varepsilon}_e$ is the host medium relative permittivity, $\sigma_a$ is a coupling strength parameter, $\overline{N}_0$ is the total dye concentration, $\tau_{jl}$ is the relaxation times for the state transitions, and $\Gamma_p = \sigma_{abs}I_p/(hf)$ is the pumping rate (with $\sigma_{abs}$ being the absorption cross-section, $I_p$ being the pump intensity, $h$ being the Planck constant, and $f$ being the pump frequency). Similar models also hold for gain materials based on quantum dots (44, 45).

The theory below, valid for the steady-state response, is derived through a time-harmonic wave-scattering formalism. Accordingly, we consider only the complex relative permittivity values at a single operational frequency, $\varepsilon_h$, $\varepsilon_i = \varepsilon'_i + i\varepsilon''_i$ and $\varepsilon_e = \varepsilon'_e + i\varepsilon''_e$, with the prime and double-prime tagging the real and imaginary parts, respectively; in view of the assumed time convention, positive and negative imaginary parts correspond to loss and gain, respectively. However, we will take into account the full dispersive models in Eqs. **1**–**3** when dealing with stability issues (*SI Appendix*).

The general theory of photonic doping of ENZ media (15) is not limited to doping particles characterized by real-valued constitutive parameters, and therefore holds for our scenario of interest. Accordingly, as depicted in Fig. 1*B*, for an exterior observer, the structure in Fig. 1*A* can be effectively replaced by a homogeneous region of the same shape and ENZ character, but exhibiting an effective (generally nonunit) relative permeability $\mu_{eff}$. For our core–shell doping particle, the effective permeability can be calculated analytically in closed form; the exact expression is not given here, for brevity, and can be found in *SI Appendix* together with its detailed derivation (*SI Appendix*, Eqs. **S1**–**S7**). To illustrate the basic idea underlying our approach, here we focus on its approximation,

$$\mu_{eff} \approx 1 + \frac{\pi k^2\left[(\varepsilon_i - \varepsilon_e)R_i^4 + \varepsilon_e R_e^4\right]}{2A\left\{4 - k^2\left[(\varepsilon_i - \varepsilon_e)R_i^2 + \varepsilon_e R_e^2\right]\right\}}, \qquad [4]$$

valid in the limit of electrically small radii $kR_{i,e} \ll 1$ (see *SI Appendix* for details). In Eq. **4**, $A$ denotes the total area (host + dopant regions) of the structure in Fig. 1*A*, and $k = \omega/c = 2\pi/\lambda$ denotes the vacuum wavenumber (with $c$ and $\lambda$ being the corresponding speed of light and wavelength, respectively). In particular, we observe that the denominator of the fraction in Eq. **4** vanishes for

$$\varepsilon_i = \varepsilon_e - \frac{\varepsilon_e R_e^2}{R_i^2} + \frac{4}{k^2 R_i^2}. \qquad [5]$$

Within the limits of the implied approximation, Eq. **5** provides a condition that the core and shell relative permittivities need to

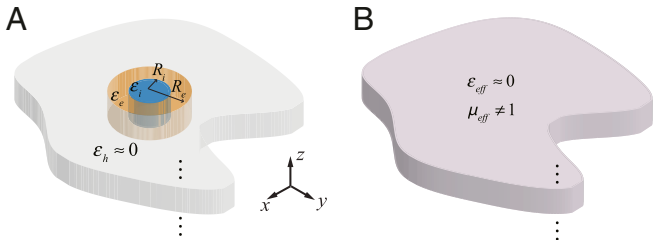


**Fig. 1.** Problem geometry. (*A*) A 2-D host region, of infinite extent along the $z$ direction, arbitrarily shaped in the $x$–$y$ plane, filled with an ENZ medium with relative permittivity $\varepsilon_h \approx 0$ is doped with a core–shell cylindrical, nonmagnetic particle with interior and exterior radii $R_i$ and $R_e$, and corresponding (complex-valued) relative permittivities $\varepsilon_i$ and $\varepsilon_e$, respectively. (*B*) For an exterior observer, the structure is effectively equivalent to a homogenous region, of identical shape and ENZ character ($\varepsilon_{eff} \approx 0$), but exhibiting an effective (generally nonunit) relative permeability $\mu_{eff}$.

fulfill in order to give rise to a pole-type singularity in the effective permeability. Interestingly, such a condition can be satisfied for real-valued frequencies also in the presence of complex-valued permittivities, that is, of suitably tailored gain and loss in the core and shell regions. This represents a key difference with respect to the cylindrical doping particle configuration considered in the original study (15), which can be recovered from Eq. **5** by assuming either $R_e = R_i$ or $\varepsilon_e = \varepsilon_i$. In this latter case, it can be readily verified that the pole condition can be satisfied for real-valued frequencies only in the absence of gain and loss.

The above reasoning is not limited to the electrically small regime; for larger structures, the complex pole condition can no longer be expressed in a simple closed form and needs to be found numerically. From a phenomenological viewpoint, such singularity implies the possibility to achieve broad tunability of the effective permeability over the entire complex plane, by changing the core and shell radii and/or the corresponding permittivities.

This is quantitatively illustrated in Fig. 2 for a parameter configuration featuring $\varepsilon_h = 0.001$, $A = 0.496\lambda^2$, $R_i = 0.14\lambda$, $R_e = 0.17\lambda$, and $\varepsilon_e = 5 - i0.5$. For these parameters, the pole condition (calculated from the exact expression of $\mu_{eff}$ in *SI Appendix*, Eq. **S7** for higher accuracy) yields $\varepsilon_i = 5.114 + i0.287$. Fig. 2*A* shows, in the complex $\varepsilon_e$ plane, a number of circles centered at the pole (magenta cross), whereas Fig. 2*B* shows the corresponding mappings (with approximate circular shapes) in the complex $\mu_{eff}$ plane, with the one-to-one correspondence illustrated via color coding. It can be observed that increasingly smaller circles (i.e., closer to the pole singularity) in the complex $\varepsilon_e$ plane are mapped onto increasingly larger circle-like curves in the complex $\mu_{eff}$ plane, thereby demonstrating the anticipated broad tunability (in sign and amplitude) of the effective permeability over the entire complex plane. Fig. 2 *C* and *D* shows two representative cuts (at fixed $\varepsilon'_e$, as a function of $\varepsilon''_e$) from which it can be observed that arbitrary combinations of positive and negative real and imaginary parts are possible, in principle. It is worth pointing out that the gain excursions considered are compatible with values attainable from the model in Eq. **3** by assuming typical parameters available in the topical literature for organic dyes (46) and quantum dots (44, 45). To give an idea, at near-infrared wavelengths, the gain level necessary to fulfill the pole condition above is compatible with the organic dye LDS798 (by Exciton), featuring $\omega_a = \omega_c = 2\pi c/\lambda_a$ (with $\lambda_a = 777$ nm), $\Delta\omega_a = 2\pi c\Delta\lambda_a/\lambda_a^2$ (with $\Delta\lambda_a = 56$ nm), $\sigma_a = 6\pi c^3\eta/(\tau_{21}\omega_a^2\sqrt{\hat{\varepsilon}_e})$ (with $\eta = 0.48$), $\overline{N}_0 = 6.1\cdot 10^{18}\text{cm}^{-3}$, $\tau_{21} = 50$ ps, $\tau_{10} = 100$ fs, $\tau_{32} = 100$ fs, and $\Gamma_p = 2.070 \times 10^9\ \text{s}^{-1}$ (46).

Moreover, we highlight that the parameters above constitute only one example that satisfies the pole condition, and that there are infinite combinations that could also work with much lower levels of gain and loss. For instance, maintaining the same geometrical and host medium parameters as above, and enforcing $\varepsilon_e = 5 - i0.05$ (i.e., an order-of-magnitude lower level of gain), we obtain, from *SI Appendix*, Eq. **S7**, $\varepsilon_i = 5.109 + i0.0287$ as an alternative pole condition.

For validation purposes, we consider a parameter configuration tailored so as to yield a targeted $\mu_{eff} = -1 - i10$, and show, in Fig. 2 *E* and *F*, the numerically (finite-element) computed near-field distributions pertaining to the actual and effective structures, respectively, excited by an elementary electric dipole. As can be observed, the field distributions in the exterior vacuum region are essentially identical, as are the corresponding (far-field) radiation patterns shown in Fig. 2*G*.

Finally, we note that, along the lines of what developed in ref. 15 for cylindrical dielectric doping particles (see supplementary note 3 therein), the lossy, dispersive character of the ENZ host in Eq. **1** could be directly incorporated in the model in terms of suitable correction factors in the effective permeability. However, in view of the more complex (core–shell) geometry considered here, such extension is rather cumbersome and less physically insightful, and we leave it to future developments.

**Application Examples.** The above premises suggest a variety of possible applications for engineering of unconventional and/or reconfigurable optical responses. For instance, the broad tunability of the effective permeability achievable by solely acting on the gain parameter (as illustrated in Fig. 2 *C* and *D*) opens up interesting perspectives in reconfigurability mechanisms based on optical pumping. As also suggested in previous related studies (16), for an easier interpretation of the optical response, it is expedient to consider slab-type configurations, as shown in Fig. 3*A*, made of periodic arrangements of square unit cells, under plane wave illumination. For such a geometry, Fig. 3*B* shows the reflectance and transmittance responses, as a function of the gain parameter $\varepsilon''_e$, for a configuration optimized so as to exhibit strong sensitivity to small variations of the gain (see *SI Appendix* for details). As can be observed in the reflectance response, around the deep minimum, variations of the gain parameter of ∼20% (which could be induced by suitable optical pumping) are sufficient to switch from an almost perfect impedance matching to a quite strong impedance mismatch, with over four-order-of-magnitude variations in the reflectance (from $\sim 10^{-4}$ to $\sim 1$). In fact, values of reflectance moderately larger than 1 (∼2.8) can be obtained with ∼30% gain variations. As shown in Fig. 3 *C* and *D*, this mechanism essentially relies on the transition from an epsilon-and-mu-near-zero (impedance matching) condition to strongly mismatched configurations characterized by significantly larger (although still small in absolute value) effective permeabilities. Fig. 3 *E* and *F* shows the field intensity distributions pertaining to two such distinct states, from which the absence and presence, respectively, of a standing wave can be observed in the incidence region.

It is worth pointing out that gain variations of the same order are much less effective in more conventional configurations that do not exhibit effective magnetism. For illustration, in *SI Appendix*, Fig. S1, we consider a benchmark bilayer configuration composed of a gain layer with relative permittivity the same as the shell material in Fig. 3 (and thickness adjusted so as to equalize the overall concentration) paired with an antireflection lossy layer, showing that gain variations of the same order as in Fig. 3 yield much milder reflectance variations, with values that always remain below ∼0.1.

Also in this case, we remark that the gain levels in Fig. 3 are in line with those attainable via organic dyes (43, 46) and quantum dots (44, 45) at infrared wavelengths. For these parameters, the gain level scales almost linearly with the pumping rate (and, hence, intensity), and, therefore, mild (∼20%) variations appear to be feasible. Moreover, alternative optimized structures operating with lower gain levels can be engineered, as illustrated in *SI Appendix*, Fig. S2.

The possibility of relying on an arbitrary complex-valued permeability enables the engineering of unconventional optical responses. For instance, it is possible to obtain signal amplification in conjunction with near-zero reflectance or transmittance.

From Fig. 3*B*, it can be verified that, at the reflectance dip, the transmittance is nearly 1, whereas the regions featuring signal amplification in transmission are characterized by strong reflectance. This is not surprising, in view of the underlying assumption of a lossless ENZ host, which implies that the impedance matching condition is fulfilled for a real-valued effective permeability (Fig. 3 *C* and *D*). In other words, loss and gain in the core–shell doping particle must exactly balance at the impedance matching condition. This constraint can be lifted by assuming that the ENZ host exhibits gain (i.e., $\varepsilon''_h < 0$). In this case, at the impedance matching condition, the signal amplification in transmission would be essentially dictated by the amplification constant

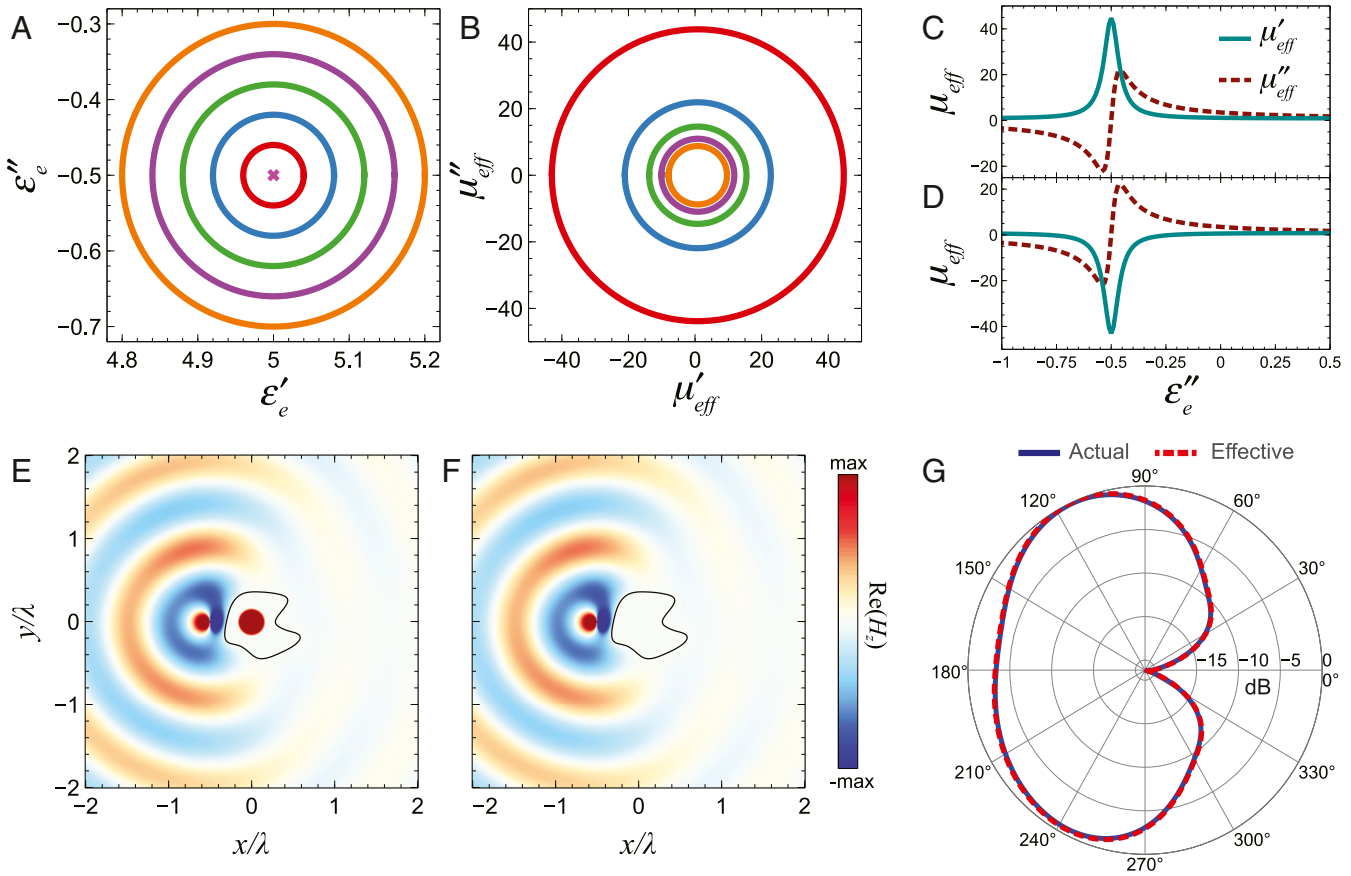


**Fig. 2.** Effective parameters. Representative results assuming $\varepsilon_h = 0.001$, $A = 0.496\lambda^2$, $R_i = 0.14\lambda$, and $R_e = 0.17\lambda$, for which the effective permeability exhibits a pole for $\varepsilon_e = 5 - i0.5$ and $\varepsilon_i = 5.114 + i0.287$. (*A*) Circular contours in the complex $\varepsilon_e$ plane centered at the pole (magenta cross). (*B*) Corresponding mapping in the complex $\mu_{eff}$ plane, with color coding illustrating the one-to-one correspondence. (*C* and *D*) Representative cuts of $\mu_{eff}$, as a function of the gain parameter $\varepsilon''_e$, for $\varepsilon'_e = 4.96$ and $\varepsilon'_e = 5.04$, respectively. (*E*) Normalized near-field map [Re($H_z$)] pertaining to a configuration with $\varepsilon_i = 5.114 + i0.287$, $\varepsilon_e = 5.030 - i0.670$, excited by an elementary, *y*-directed electric dipole placed at $x = -0.5\lambda$, $y = 0$. (*F*) Corresponding results for a homogeneous configuration with effective parameters $\varepsilon_{eff} = 0.001$, $\mu_{eff} = -1 - i10$. (*G*) Comparison between the corresponding radiation patterns, normalized with respect to the maximum radiated intensity.

$kL\sqrt{-\varepsilon''_h}$. This implies that, for small to moderately sized layers, sensible amplification generally require gain levels that, while not necessarily large in absolute value, may invalidate the underlying ENZ assumption and, in turn, the analytic derivations of the closed-form effective parameters $\varepsilon_{eff} = \varepsilon_h$ and $\mu_{eff}$ given in Eq. **4** (and *SI Appendix*, Eq. **S7**). To give an idea, in *SI Appendix*, Fig. S3, we compare the theoretical effective parameters for a configuration featuring $\varepsilon_h = 0.01 - i0.01$ with the values obtained from a conventional parameter retrieval algorithm (47). As can be observed, the differences may be substantial, up to a factor of ∼4. Nevertheless, it is important to emphasize that the doping principle remains valid also in this regime, as the structure still exhibits effective magnetism, even though the magnetic field in the ENZ region may not be uniform, and the effective properties may depend on the dopant location and not be accurately expressed analytically in closed form. Fig. 4*A* shows the response of a structure that was numerically optimized so as to exhibit the desired response. The optimization was carried out directly in the space of the physical ($\varepsilon_h$, $\varepsilon_i$, $\varepsilon_e$) and geometrical ($R_i$, $R_e$) parameters, without resorting to the analytic effective parameter representation (see *SI Appendix* for details). As can be observed, for a specific value of the gain level in the shell region, it exhibits a transmittance of ∼5 accompanied by near-zero reflectance; the corresponding field distribution is shown in Fig. 4*B*. Similar to the previous example, the gain parameter $\varepsilon''_e$ can be exploited to tune (via optical pumping) the reflectance response over several orders of magnitude, while maintaining an essentially constant transmittance. The extracted effective parameters are shown in *SI Appendix*, Fig. S4; as expected, at the impedance matching condition, the imaginary parts are negative. Also in this case, it is interesting to compare the response with that of a conventional nonmagnetic bilayer structure consisting of a gain material layer (with the same permittivity and concentration as the shell material in Fig. 4*A*) paired with an antireflection lossy layer. As shown in *SI Appendix*, Fig. S5, in this case, the transmittance is much lower (over an order of magnitude), thereby indicating the pivotal role played by the effective magnetism (and, hence, doping) in our proposed configuration.

Concerning the dual response, that is, signal amplification in reflection and near-zero transmission, a straightforward implementation may feature a gain material layer backed by a regular photonic-doped ENZ layer tuned so as to exhibit a perfect magnetic conductor response (15). However, it is possible and insightful to engineer this response with a single layer of active ENZ material doped with non-Hermitian core–shell particles. As shown in *SI Appendix*, Fig. S6 and the accompanying discussion, effective magnetism accompanied by gain allows unconventional tradeoffs between reflectance and transmittance, including the response of interest here. However, also in this case, it is necessary to operate in a parameter regime where the closed-form expressions for the effective parameters are not applicable, and therefore the structure needs to be optimized

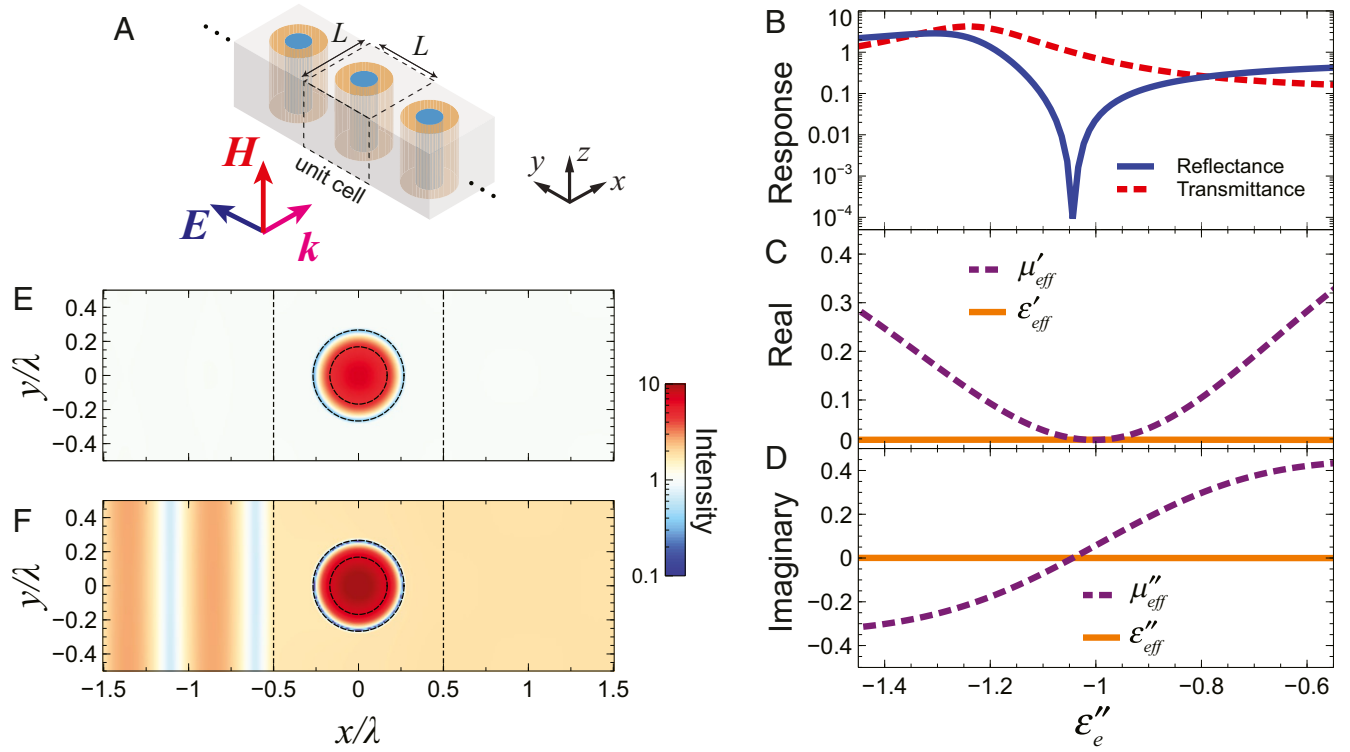


**Fig. 3.** Reconfigurable reflection. (*A*) Slab-type configuration, of infinite extent along the *z* direction, and with periodic arrangement of square unit cells of side length *L* along the *y* direction, under transverse magnetic plane wave illumination. (*B*) Reflectance and transmittance responses, as a function of the gain parameter $\varepsilon''_e$, for an optimized parameter configuration with $\varepsilon_h = 0.001$, $L = \lambda$, $R_i = 0.178\lambda$, $R_e = 0.281\lambda$, $\varepsilon_i = 2.005 + i2.560$, and $\varepsilon'_e = 2.721$. (*C* and *D*) Corresponding real and imaginary parts of effective parameters, respectively. (*E* and *F*) Field intensity ($|H_z|^2$) maps (normalized with respect to impinging intensity) across the unit cell for $\varepsilon''_e = -1.044$ (impedance matching) and $\varepsilon''_e = -1.305$ (strong impedance mismatch), respectively.

directly in the physical/geometrical parameter space. Fig. 4*C* shows an example of an optimized structure which, for varying level of gain in the core ($\varepsilon''_i$), exhibits an almost flat reflectance of ~2.8 and a moderately tunable transmittance that can be as low as $\sim 10^{-8}$, thereby yielding an almost perfect amplifying mirror. The corresponding field distribution is shown in Fig. 4*D*, whereas the extracted parameters are shown in *SI Appendix*, Fig. S7.

We now move on to a different non-Hermitian scenario, schematized in Fig. 5*A*, featuring an ENZ bilayer with loss ($\varepsilon = \varepsilon_h = \varepsilon'_h + i\varepsilon''_h$, $\varepsilon''_h > 0$) on one side and gain ($\varepsilon = \varepsilon_h^* = \varepsilon'_h - i\varepsilon''_h$) on the other, periodically doped with identical cylindrical (lossless) dielectric particles. Note that the host permittivity distribution obeys the PT symmetry condition (22, 23)

$$\varepsilon(x, -y) = \varepsilon^*(x, y), \qquad [6]$$

and this condition is preserved also in the presence of the lossless doping particles, provided that they are placed symmetrically across the gain–loss interface $y = 0$.

As summarized in *SI Appendix*, PT-symmetric gain–loss interfaces like the one in Fig. 5*A* can sustain surface waves resembling surface plasmon polaritons, which are exponentially bound along the *y* direction and propagate unattenuated along the *x* direction (33, 34, 48). This waveguiding mechanism can be sustained in the presence of a sufficiently high gain/loss level $\varepsilon''_h$, and becomes progressively less effective for reduced gain/loss levels, eventually transitioning to a leaky-type radiation mechanism below a certain threshold (34). However, we showed, in a previous study (34), that, in the ENZ regime, such a gain/loss threshold can be significantly lowered (see also *SI Appendix* for details). The above physical mechanism, in principle, enables very intriguing "on-demand" waveguiding effects, for instance, by deploying in a lossy background channels made of gain media, and activating them selectively via suitable optical pumping. To add further complexity and new degrees of freedom, we explore the effects of effective magnetism induced by photonic doping. As shown in *SI Appendix*, unlike the previous scenario in Fig. 1*A*, here, there is no apparent advantage in assuming a non-Hermitian core–shell doping particle, so we consider a standard photonic doping as in the original study (15). However, the presence of a PT-symmetric ENZ host implies two characteristics that render the extension of the general theory not straightforward: 1) the presence of an interface between two doped regions and 2) the generally non-constant (in fact, exponentially decaying for the surface wave scenario of interest) magnetic field distribution inside the ENZ bilayer.

We first consider a configuration in the absence of doping (and hence of effective magnetism), with parameters $\varepsilon_h = 10^{-5} + i10^{-3}$ and $d = 0.25\lambda$, chosen so that the waveguiding mechanism cannot be sustained (gain/loss threshold level of $4.4 \cdot 10^{-3}$; see *SI Appendix* for details). Although such low losses (and small gain, for $\varepsilon_h^* = 10^{-5} - i10^{-3}$) are not available in natural ENZ materials, they can be, in principle, attained via suitable loss compensation (37, 42). From the intensity map in Fig. 5*B*, and the corresponding transverse cut in Fig. 5*G*, it is apparent that the field is not confined inside the bilayer, but it is rather radiated in the exterior vacuum region. As detailed in *SI Appendix*, for the same gain/loss level, a magnetic response could render the waveguiding mechanism much more effective. For instance, Fig. 5*C* shows the ideal response of a bilayer with the same permittivity distribution as above, but now with a relative permeability $\mu = 25$. The presence of a bound mode at the gain–loss interface is now evident, with the standing wave pattern attributed to the structure truncation along the *x* direction. The exponential localization at the gain–loss interface is better visualized in the transverse cut shown in Fig. 5*F*.

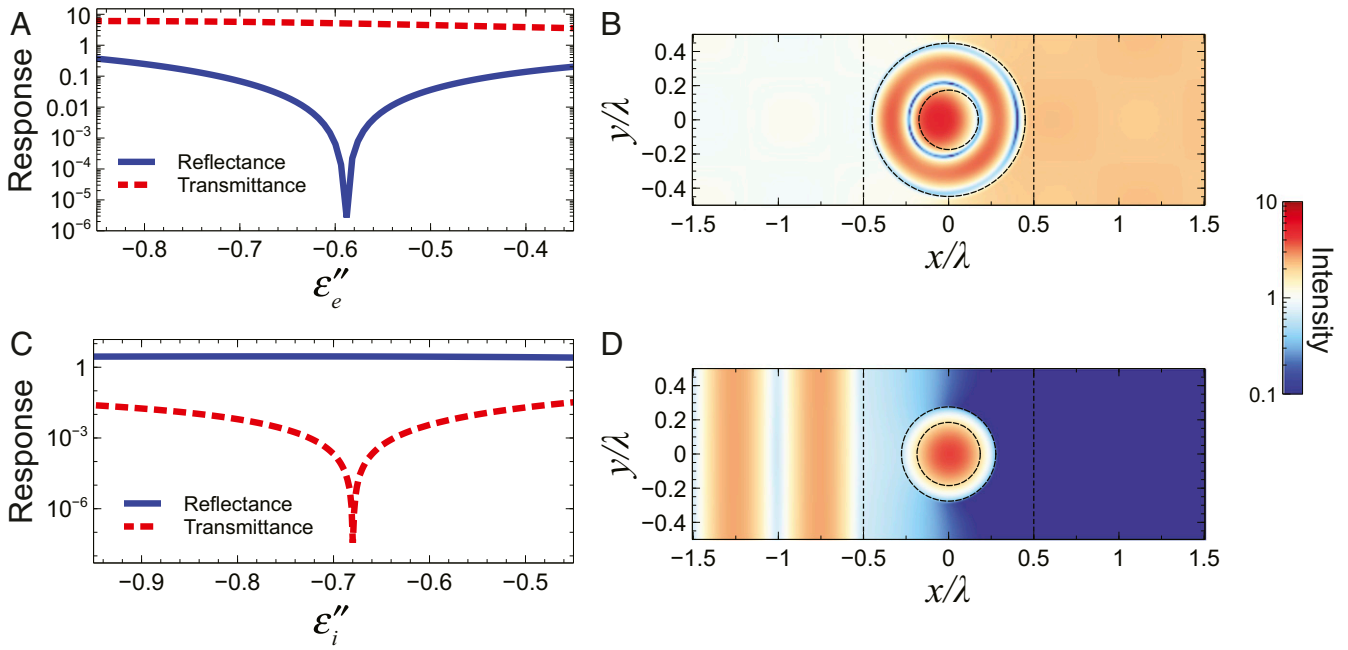


**Fig. 4.** Signal amplification with near-zero reflection or transmission. Geometry as in Fig. 3*A*, with $L = \lambda$. (*A*) Reflectance and transmittance responses, as a function of the gain parameter $\varepsilon''_e$, for an optimized parameter configuration with $\varepsilon_h = 0.01 - i0.01$, $R_i = 0.183\lambda$, $R_e = 0.472\lambda$, $\varepsilon_i = 2.212 + i0.366$, and $\varepsilon'_e = 5.242$, behaving as an impedance-matched amplifier. (*B*) Field intensity ($|H_z|^2$) map (normalized with respect to impinging intensity) across the unit cell for $\varepsilon''_e = -0.588$ (impedance matching). (*C*) Reflectance and transmittance responses, as a function of the gain parameter $\varepsilon''_i$, for an optimized parameter configuration with $\varepsilon_h = 0.01 - i0.0480$, $R_i = 0.195\lambda$, $R_e = 0.290\lambda$, $\varepsilon'_i = 2.051$, and $\varepsilon_e = 1.680 + i0.159$, behaving as an amplifying mirror. (*D*) Field intensity ($|H_z|^2$) map (normalized with respect to impinging intensity) across the unit cell for $\varepsilon''_i = -0.680$ (minimum transmittance). The black dashed circles and lines delimit the core–shell and unit cell regions, respectively. The effective parameters for these two configurations are shown in *SI Appendix*, Figs. S4 and S7, respectively.

The next step is to realize the magnetic response via photonic doping. For the assumed parameters, the general theory (15) is applicable, and, by inverting the closed-form expression of the effective permeability, we obtain the doping particle parameters $\varepsilon_d = 11.9$, $R_d = 0.11\lambda$. Fig. 5*D* shows the corresponding intensity distribution, from which the field confinement at the gain–loss interface is apparent. For a more quantitative assessment, Fig. 5*F* compares a transverse cut with that pertaining to the ideal ($\mu = 25$) scenario, showing a very good agreement. This indicates that the photonic doping concept is also applicable in the presence of interfaces and fast variations of the magnetic field distribution.

It is worth stressing that, although their level is quite low ($\varepsilon''_h = 10^{-3}$), gain and loss are essential for the above waveguiding mechanism. To gain some insight, Fig. 5 *E* and *G* shows the intensity map and the transverse cut, respectively, pertaining to the same doping scenario as in Fig. 5*F*, but now with the gain switched to zero (and loss still present). Despite the still visible doping effect, the exponential localization at the interface is now totally lost, and the field distribution is completely extended in the transverse direction. Once again, the possibility of switching from a completely extended to an exponentially bound field distribution (possibly with subwavelength localization) via (de) activation of a very small level of gain is particularly intriguing for potential applications in reconfigurable nanophotonics.

We note that the above configuration differs fundamentally from other coupled chains of gain/loss particles, which can also sustain waveguiding mechanisms (49). One important difference is the sensitivity to the doping particle displacement, as a consequence of the generally nonconstant magnetic field distribution in the ENZ host regions. In *SI Appendix*, Fig. S8, we show that the waveguiding mechanism is quite robust with respect to particle displacements that preserve the PT symmetry condition in Eq. **6**, whereas it is very sensitive to displacements that break it. This strong sensitivity could be exploited for engineering interesting mechanical actuation systems and for optical sensing purposes.

## Discussion

The above results provide an interesting extension of the concept of photonic doping of ENZ media (15) to non-Hermitian scenarios featuring suitably tailored distributions of loss and gain either in the doping particles or in the ENZ host medium. Specifically, they bring about an additional dimensionality, granting access to the entire complex plane for the synthesis of the effective permeability. This may open up interesting vistas in the emerging fields of non-Hermitian optics and photonics (22–24), especially in conjunction with design approaches such as complex coordinate transformation optics (50, 51), which inherently rely on materials with complex-valued permeability. Moreover, the possibility of tuning the effective permeability by varying the gain (e.g., via optical pumping), thereby switching between different optical responses (e.g., low/high reflectance and bound/extended field distribution), may find interesting applications in reconfigurable nanophotonics.

Our findings also indicate that the range of applicability of the photonic doping concept can be extended to scenarios featuring moderate departures from the ENZ host assumption, the presence of interfaces between two host media, and nonconstant magnetic field distributions.

Although an experimental realization is beyond the scope of this theoretical study, and no specific materials have been identified for a practical implementation, the design optimization in the application examples has been constrained (see *SI Appendix* for details) so as to yield realistic gain levels, in line with those attainable via organic dyes (43, 46) and quantum dots (44, 45). When dealing with active materials, it is important to be aware of the possible occurrence of optical instability, in the form of self-oscillations that can be supported by the system. In related studies

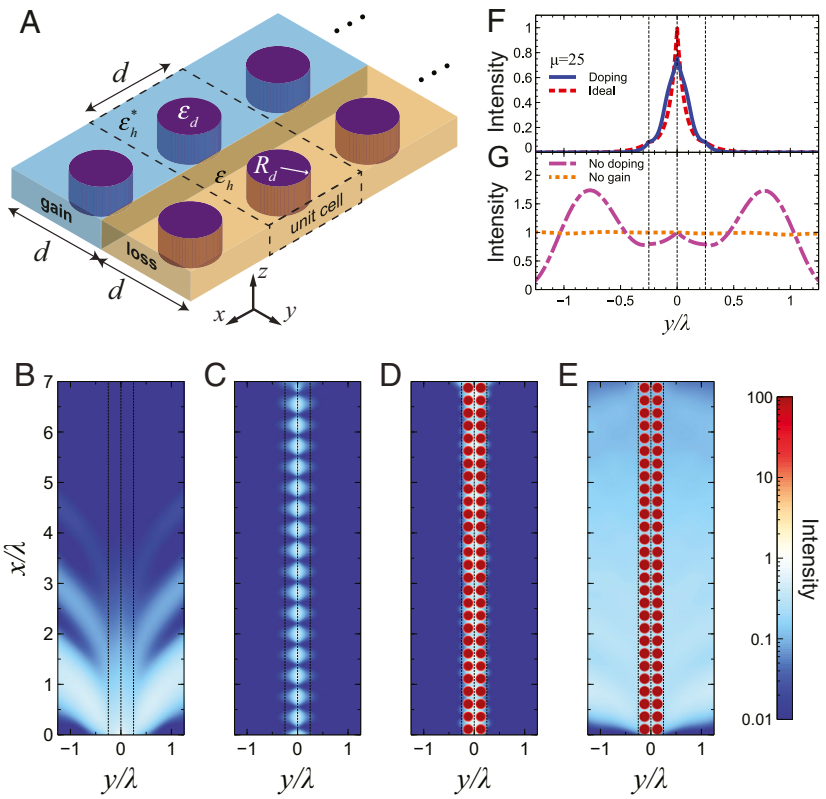


**Fig. 5.** Waveguiding at gain–loss interfaces. (*A*) Geometry of a PT-symmetric gain–loss bilayer, with $\varepsilon_h = 10^{-5} + i10^{-3}$, $d = 0.25\lambda$, periodically doped with cylindrical dielectric particles with radius $R_d$ and relative permittivity $\varepsilon_d$. The structure is assumed to be of infinite extent along the $z$ direction, and periodic (with square unit cell of side length $d$) along the $x$ direction. (*B*) Field intensity ($|H_z|^2$) map in the absence of doping (and hence of effective magnetism). (*C*–*E*) Corresponding field maps by assuming a relative permeability $\mu = 25$, photonic doping with $\varepsilon_d = 11.9$, $R_d = 0.11\lambda$ (corresponding to an effective relative permeability $\mu_{eff} = 25$), and the same photonic doping but in the absence of gain in the host medium. The black-dashed lines delimit the bilayer region. (*F* and *G*) Transverse cuts at $x = 4\lambda$, pertaining to the maps in *B* and *C* and *D* and *E*, respectively.

dealing with cylindrical non-Hermitian configurations (38, 52), it has been shown that unconditional stability could be, in principle, attained by suitably tailoring the dispersion properties of the material constituents. In *SI Appendix*, Fig. S9, we address this issue in detail for a specific example and for a realistic model of the gain medium. We show that unconditional stability is, in principle, achievable even in the presence of moderately large negative values of the effective permeability imaginary part.

Current and future studies are aimed at exploring other interesting non-Hermitian scenarios, for example, involving exceptional points and spectral singularities, as well as leveraging the photonic doping concept within the framework of complex coordinate transformation optics (50, 51). Also of great interest is the extension of the analytic model so as to incorporate the lossy characteristics of the ENZ host, along the lines of what developed in ref. 15 for the Hermitian scenario.

## Methods

The numerical simulations in our study were carried out by means of the radio frequency module available in the finite-element-based commercial software package COMSOL Multiphysics (https://www.comsol.com/comsol-multiphysics). Specifically, for the simulations in Figs. 2 *E* and *F* and 5 (as well as *SI Appendix*, Fig. S8), the computational domain is terminated by perfectly matched layers. The scattering patterns in Fig. 2*G* are obtained via near-to-far-field transformation by means of the embedded farfield option. The structures in Fig. 5 and *SI Appendix*, Fig. S8 are excited via an impressed magnetic field distribution that matches the ideal guided mode distribution in Fig. 5*C*. For the simulations in Figs. 3 and 4 (as well as *SI Appendix*, Figs. S2–S4 and S7), the unit cell is terminated by periodic Bloch-type boundary conditions along the $x$ direction, whereas port-type terminations are assumed along the incidence direction $y$. For all simulations, an adaptive meshing is utilized with triangular elements and maximum element size of a hundredth of the ambient wavelength. Moreover, the MUltifrontal Massively Parallel Sparse direct Solver (MUMPS) is utilized with default parameters.

**Data Availability.** All data needed to evaluate the conclusions in the paper are available in the manuscript and *SI Appendix*.

**ACKNOWLEDGMENTS.** This work was supported in part by the Italian Ministry for Education, University and Research through the Funding for Basic Activities Related to Research, and by the University of Sannio through the Fondo di Ricerca di Ateneo program. N.E. acknowledges partial support from the Vannevar Bush Faculty Fellowship program sponsored by the Basic Research Office of the Assistant Secretary of Defense for Research and Engineering and funded by the Office of Naval Research through Grant N00014-16-1-2029.

1. F. Capolino, *Theory and Phenomena of Metamaterials*, (CRC, 2009).
2. W. Cai, V. M. Shalaev, *Optical Metamaterials: Fundamentals and Applications*, (Springer, 2010).
3. M. Silveirinha, N. Engheta, Tunneling of electromagnetic energy through subwavelength channels and bends using ε-near-zero materials. *Phys. Rev. Lett.* **97**, 157403 (2006).
4. I. Liberal, A. M. Mahmoud, N. Engheta, Geometry-invariant resonant cavities. *Nat. Commun.* **7**, 10989 (2016).
5. F. Monticone, A. Alù, Embedded photonic eigenvalues in 3D nanostructures. *Phys. Rev. Lett.* **112**, 213903 (2014).
6. M. G. Silveirinha, Trapping light in open plasmonic nanostructures. *Phys. Rev. A* **89**, 23813 (2014).
7. S. Lannebère, M. G. Silveirinha, Optical meta-atom for localization of light with quantized energy. *Nat. Commun.* **6**, 8766 (2015).
8. O. Reshef, I. D. Leon, M. Z. Alam, R. W. Boyd, Nonlinear optical effects in epsilon-near-zero media. *Nat. Rev. Mater.* **4**, 535–551 (2019).
9. E. Nahvi, I. Liberal, N. Engheta, Nonperturbative effective magnetic nonlinearity in ENZ media doped with Kerr dielectric inclusions. *ACS Photonics* **6**, 2823–2831 (2019).

10. A. R. Davoyan, A. M. Mahmoud, N. Engheta, Optical isolation with epsilon-near-zero metamaterials. *Opt. Express* **21**, 3279–3286 (2013).
11. R. Fleury, A. Alù, Enhanced superradiance in epsilon-near-zero plasmonic channels. *Phys. Rev. B* **87**, 201101 (2013).
12. I. Liberal, N. Engheta, The rise of near-zero-index technologies. *Science* **358**, 1540–1541 (2017).
13. I. Liberal, N. Engheta, Near-zero refractive index photonics. *Nat. Photonics* **11**, 149–158 (2017).
14. X. Niu, X. Hu, S. Chu, Q. Gong, Epsilon-near-zero photonics: A new platform for integrated devices. *Adv. Opt. Mater.* **6**, 1701292 (2018).
15. I. Liberal, A. M. Mahmoud, Y. Li, B. Edwards, N. Engheta, Photonic doping of epsilon-near-zero media. *Science* **355**, 1058–1062 (2017).
16. I. Liberal, Y. Li, N. Engheta, Reconfigurable epsilon-near-zero metasurfaces via photonic doping. *Nanophotonics* **7**, 1117–1127 (2018).
17. B. Jin, C. Argyropoulos, Nonreciprocal transmission in nonlinear PT-symmetric metamaterials using epsilon-near-zero media doped with defects. *Adv. Opt. Mater.* **7**, 1901083 (2019).
18. N. Liu *et al*., Enhancing the magneto-optical effects in low-biased gyromagnetic media via photonic doping. *Opt. Lett.* **44**, 3050–3053 (2019).
19. I. Liberal, N. Engheta, Zero-index structures as an alternative platform for quantum optics. *Proc. Natl. Acad. Sci. U.S.A.* **114**, 822–827 (2017).
20. Y. Zhang, Y. Luo, J. B. Pendry, B. Zhang, Transformation-invariant metamaterials. *Phys. Rev. Lett.* **123**, 67701 (2019).
21. C. M. Bender, S. Boettcher, Real spectra in non-Hermitian Hamiltonians having PT symmetry. *Phys. Rev. Lett.* **80**, 5243–5246 (1998).
22. L. Feng, R. El-Ganainy, L. Ge, Non-Hermitian photonics based on parity–time symmetry. *Nat. Photonics* **11**, 752–762 (2017).
23. R. El-Ganainy *et al*., Non-Hermitian physics and PT symmetry. *Nat. Phys.* **14**, 11–19 (2018).
24. R. El-Ganainy, M. Khajavikhan, D. N. Christodoulides, S. K. Ozdemir, The dawn of non-Hermitian optics. *Commun. Phys.* **2**, 37 (2019).
25. M. Miri, A. Alù, Exceptional points in optics and photonics. *Science* **363**, eaar7709 (2019).
26. S. K. Özdemir, S. Rotter, F. Nori, L. Yang, Parity-time symmetry and exceptional points in photonics. *Nat. Mater.* **18**, 783–798 (2019).
27. R. Fleury, D. L. Sounas, A. Alù, Negative refraction and planar focusing based on parity-time symmetric metasurfaces. *Phys. Rev. Lett.* **113**, 23903 (2014).
28. D. L. Sounas, R. Fleury, A. Alù, Unidirectional cloaking based on metasurfaces with balanced loss and gain. *Phys. Rev. Appl.* **4**, 14005 (2015).
29. A. Mostafazadeh, Spectral singularities of complex scattering potentials and infinite reflection and transmission coefficients at real energies. *Phys. Rev. Lett.* **102**, 220402 (2009).
30. Y. Jin, S. Xiao, N. A. Mortensen, S. He, Arbitrarily thin metamaterial structure for perfect absorption and giant magnification. *Opt. Express* **19**, 11114–11119 (2011).
31. L. Sun, S. Feng, X. Yang, Loss enhanced transmission and collimation in anisotropic epsilon-near-zero metamaterials. *Appl. Phys. Lett.* **101**, 241101 (2012).
32. S. Feng, K. Halterman, Coherent perfect absorption in epsilon-near-zero metamaterials. *Phys. Rev. B* **86**, 165103 (2012).
33. S. Savoia, G. Castaldi, V. Galdi, A. Alù, N. Engheta, Tunneling of obliquely incident waves through PT-symmetric epsilon-near-zero bilayers. *Phys. Rev. B* **89**, 85105 (2014).
34. S. Savoia, G. Castaldi, V. Galdi, A. Alù, N. Engheta, PT-symmetry-induced wave confinement and guiding in ε-near-zero metamaterials. *Phys. Rev. B* **91**, 115114–10 (2015).
35. J. Luo, B. Liu, Z. H. Hang, Y. Lai, Coherent perfect absorption via photonic doping of zero-index media. *Laser Photonics Rev.* **12**, 1800001 (2018).
36. J. Luo, J. Li, Y. Lai, Electromagnetic impurity-immunity induced by parity-time symmetry. *Phys. Rev. X* **8**, 31035 (2018).
37. Y. Li, C. Argyropoulos, Exceptional points and spectral singularities in active epsilon-near-zero plasmonic waveguides. *Phys. Rev. B* **99**, 75413 (2019).
38. M. Moccia, G. Castaldi, A. Alu, V. Galdi, Harnessing spectral singularities in non-Hermitian cylindrical structures. *IEEE Trans. Antenn. Propag.* **68**, 1704–1716 (2020).
39. J. Kim *et al*., Role of epsilon-near-zero substrates in the optical response of plasmonic antennas. *Optica* **3**, 339–346 (2016).
40. P. R. West *et al*., Searching for better plasmonic materials. *Laser Photonics Rev.* **4**, 795–808 (2010).
41. M. H. Javani, M. I. Stockman, Real and imaginary properties of epsilon-near-zero materials. *Phys. Rev. Lett.* **117**, 107404 (2016).
42. S. Campione, F. Capolino, Composite material made of plasmonic nanoshells with quantum dot cores: Loss-compensation and ε-near-zero physical properties. *Nanotechnology* **23**, 235703 (2012).
43. S. Campione, M. Albani, F. Capolino, Complex modes and near-zero permittivity in 3D arrays of plasmonic nanoshells: Loss compensation using gain. *Opt. Mater. Express* **1**, 1077–1089 (2011).
44. I. Moreels, D. Kruschke, P. Glas, J. W. Tomm, The dielectric function of PbS quantum dots in a glass matrix. *Opt. Mater. Express* **2**, 496–500 (2012).
45. S. D. Campbell, R. W. Ziolkowski, The performance of active coated nanoparticles based on quantum-dot gain media. *Adv. Optoelectron.* **2012**, 1–6 (2012).
46. V. Caligiuri, L. Pezzi, A. Veltri, A. De Luca, Resonant gain singularities in 1D and 3D metal/dielectric multilayered nanostructures. *ACS Nano* **11**, 1012–1025 (2017).
47. D. R. Smith, D. C. Vier, T. Koschny, C. M. Soukoulis, Electromagnetic parameter retrieval from inhomogeneous metamaterials. *Phys. Rev. E Stat. Nonlin. Soft Matter Phys.* **71**, 36617 (2005).
48. S. Savoia, G. Castaldi, V. Galdi, Non-Hermiticity-induced wave confinement and guiding in loss-gain-loss three-layer systems. *Phys. Rev. A* **94**, 43838 (2016).
49. M. A. K. Othman, V. Galdi, F. Capolino, Exceptional points of degeneracy and PT symmetry in photonic coupled chains of scatterers. *Phys. Rev. B* **95**, 104305 (2017).
50. G. Castaldi, S. Savoia, V. Galdi, A. Alù, N. Engheta, PT metamaterials via complex-coordinate transformation optics. *Phys. Rev. Lett.* **110**, 173901 (2013).
51. S. Savoia, G. Castaldi, V. Galdi, Complex-coordinate non-Hermitian transformation optics. *J. Opt.* **18**, 1–13 (2016).
52. S. Savoia *et al*., Magnified imaging based on non-Hermitian nonlocal cylindrical metasurfaces. *Phys. Rev. B* **95**, 115114 (2017).